Applied Catalysis B: Environmental 204 (2017) 185–199

Contents lists available at ScienceDirect

Applied Catalysis B: Environmental

journal homepage: www.elsevier.com/locate/apcatb

One-pot synthesis of a high performance chitosan-nickel oxyhydroxide nanocomposite for glucose fuel cell and electro-sensing applications

Gumaa A. El-Nagar[a,b,*], Igor Derr[b], Abdulmonem Fetyan[b], Christina Roth[b,*]

[a] Chemistry Department, Faculty of Science, Cairo University, Cairo 12613, Egypt
[b] Institute for Chemistry and Biochemistry, FU Berlin, Takustr. 3, D-14195 Berlin, Germany

ARTICLE INFO

Article history:
Received 5 September 2016
Received in revised form
11 November 2016
Accepted 15 November 2016
Available online 16 November 2016

Keywords:
Nanocomposites
Electro-sensing
Fuel cells
Nano-chitosan
β-NiOOH
ORR
OER

ABSTRACT

This study introduces an alternative promising Pt-free catalyst of chitosan-nickel oxyhydroxide nanocomposite (nano-CS-NiOOH) with outstanding activity and durability towards glucose electrooxidation (Gox) and oxygen reduction reaction (ORR) compared to precious metal-based catalysts. Nano-CS-NiOOH modified glassy carbon (GC) electrode (nano-CS-NiOOH/GC) exhibits superb electrocatalytic activity, molecular selectivity and long-term durability for Gox. For instance, nano-CS-NiOOH/GC electrode shows ca. 10 times higher electrocatalytic activity and stability for Gox compared to nano-NiOOH/GC electrode with the same NiOOH weight. Additionally, the nano-CS-NiOOH/GC electrode exhibits a glucose sensitivity of 687 $\mu A\,mM^{-1}\,cm^{-2}$, which is 34-fold greater than that obtained at the nano-NiOOH/GC electrode ($20\,\mu A\,mM^{-1}\,cm^{-2}$) with lowest detection limit of 20 nM based on a signal-to-noise ratio of 3 and a linear range up to 8 mM. Furthermore, nano-CS-NiOOH/GC electrode showed a superior electrocatalytic activity and durability for both ORR and OER in alkaline medium compared to the commercial Pt/C electrode making it a high-performance non-precious metal-based bifunctional catalyst. NiOOH is believed to play a crucial role as a catalytic mediator to facilitate the charge transfer and chitosan is thought to enhance the catalytic activity and durability via stabilizing β-NiOOH and improving the adsorption of active species through its $-NH_2$ and —OH like functionalities.

1. Introduction

Tremendous efforts have been made to find a new renewable, eco-friendly and efficient energy resource in order to combat the conflicting rises in the global energy demand. Increased consumption and depletion of fossil fuel energy resources are discussed in the light of growing environmental concerns due to the environmental impacts of using petroleum-based energy, such as climate change and CO_2 emissions. In this regard, fuel cells (FCs) have attracted significant attention as a promising highly efficient and low emission alternative energy technology to replace the traditional power sources [1–6]. Direct glucose fuel cells (DGFCs) have received remarkable consideration as promising alternative energy sources with highly stable continuous power output through coupling of the glucose oxidation reaction (Gox) at the anode and oxygen reduction reaction (ORR) at the cathode for use in the future. Glucose fuel cells hold great promise due to the unique features of glucose as a fuel, which is renewable, cheap, non-toxic, easy to store and transport, eco-friendly and the most abundant monosaccharide in nature. Glucose is capable of releasing 2.87 MJ mol^{-1} energy upon complete oxidation to CO_2 [7–14]. Thus, development of a suitable catalyst is a vital issue due to the high overpotential associated with multiple-electron transfer steps involved in Gox (anodic reaction of DGFCs) and the sluggish kinetics of ORR (essential cathodic reaction of all polymer electrolyte membrane fuel cells). The typical enzyme catalysts used in DGFC for Gox and ORR with excellent selectivity and high activity are glucose oxidase and laccase, respectively. However, enzymatic glucose fuel cells are suffering from a major drawback; they are susceptible to the operating environment upon long-term running, due to the fragile nature of the enzymes and poor immobilization techniques [15–18]. In recent years, extensive investigation efforts have been made to study glucose as fuel for microbial fuel cells (MFC), direct fuel cells and enzymatic fuel cells. However, up-to-date, the reported electrical power outputs and stabilities are very low [7,10]. Consequently, precious-metal

* Corresponding authors.
E-mail addresses: elnagar087@yahoo.com (G.A. El-Nagar), christina.roth@fu-berlin.de (C. Roth).

http://dx.doi.org/10.1016/j.apcatb.2016.11.031
0926-3373/

based electrocatalysts (*e.g.*, Pt, Au, or their alloys) have been used to generate more electricity due to their considerable activity for Gox and ORR. But their low availability and long-term durability due to the poisoning effect of carbohydrate oxidation intermediates, besides their high cost impede their further development [7,16]. Accordingly, there are many studies which focus on finding an ideal catalyst to improve the DGFCs performance. Development of noble-metal free catalysts (e.g., metal oxide based catalysts) is a good alternative approach to reduce the cost and enhance catalytic activities and stabilities of DGFCs [19,20].

Several mechanisms of alcohol oxidation on nickel-based electrodes have been reported [21–23]. While Fleischmann et al. [22,24] proposes a catalytic mediator role of $Ni(OH)_2$/NiOOH transformations, others [23] reported that alcohol oxidation takes place after complete conversion of $Ni(OH)_2$ to NiOOH in the course of an anodic potential sweep. Thus, we assume that a portion of the anodic current is due to glucose oxidation by NiOOH and a part of the current is due to the direct glucose electrooxidation on the surface of the oxide layer. The previously published articles indicated that nickel oxide modified electrodes can catalyze the electrooxidation of glucose to gluconolactone [25,26] due to the existence of Ni (II) ions according to the following equations:

$$Ni(OH)_2 \leftrightarrow \beta - NiOOH + H^+ + e^- \quad (1)$$

$$Ni(OH)_2 + OH^- \leftrightarrow \gamma - NiOOH + H_2O + e^- \quad (2)$$

$$NiOOH + \ Glucose \leftrightarrow Ni(OH)_2 + Gluconolactone \quad (3)$$

Firstly, $Ni(OH)_2$ is transferred to NiOOH via a proton diffusion mechanism, in which most likely β-NiOOH is formed (Eq. (1)) and/or by a solvent mechanism, in which γ-NiOOH is formed through the diffusion of OH^- (Eq. (2)). Then, glucose is oxidized on the active NiOOH phase (N.B., gluconolactone [25,26] as well as methanoates and oxalates [21,27,28] have been reported as the oxidation products of glucose electrooxidation).

Glucose electrocatalysis is a topic of great practical and analytical interest. It is not only of importance for new blood glucose monitoring sensors development for clinical diagnosis and private healthcare, but also offers solutions in food monitoring, control of bioprocesses, fuel cells and pharmaceutical analysis. It has attracted tremendous academic and commercial efforts in order to develop a glucose sensor with a high sensitivity, excellent selectivity, good reliability, fast response, and low cost. Although there are a few potential glucose sensing devices including acoustic, optical, and transdermal technologies being discovered, electrochemical sensors are still known commonly as the most appropriate and effective tool for glucose analysis up to date. This is due to their many attractive features such as preeminent sensitivity, time efficiency, simple instrumentation, easy operation, and low production cost [29,30].

Among natural polymers, polysaccharides are among the best candidates due to their abundance in the environment. Chitosan (CS) is a polysaccharide natural-biopolymer, which is obtained from chitin deacetylation, and the major component of the shell of crab and shrimp. It is the second most abundant natural polysaccharide present on the earth next to cellulose. CS has been attracting considerable interest for a broad range of applications, due to its unique properties including nontoxicity, biocompatibility, and biodegradability [31]. It should be mentioned that there are a few reports on using chitosan modified GC electrode for electrocatalysis applications. For example, a nano-composite of platinum-chitosan was prepared by electrochemical co-deposition at a GC surface and used as a nitrite sensor [32], while a screen-printed chitosan-modified carbon electrode was used as a working electrode for the determination of selected metals [33]. Taufik et al. [34] reported nano Bi_2O_3/chitosan-modified gold electrode as a biosensor for DNA hybridization and nanocomposites of chitosan-reduced graphene oxide–nickel nanoparticles (CS-RGO—NiNPs) co-deposited cathodically onto a screen-printed electrode (SPE) were used as a non-enzymatic glucose electro-sensor [35,36].

Herein, a novel electrocatalyst based on nickel oxyhydroxide-chitosan nanocomposite with a high electrocatalytic activity and stability for glucose oxidation (Gox), oxygen reduction (ORR) and oxygen evolution (OER) in addition to a high sensitivity and selectivity for glucose electro-sensing was investigated. To the best of our knowledge, this is the first report on the electrochemical properties of the as-prepared nanocomposite for fuel cell applications, which up to now was known as a product generated and utilized in the adsorption process to remove heavy metals such as nickel, iron and copper ions from aqueous solutions by different types of chitosan bio-sorbents.

2. Experimental

2.1. Chemicals

Chitosan (CS) [poly-β(1–4)-2-amino-2-deoxy-D-glucose] (molecular weight 110,000–150,000, purity ≥93%), acetic acid, nickel sulfate hexahydrate ($NiSO_4 \cdot 6H_2O$, ≥99%), sodium hydroxide and glucose were obtained from Sigma-Aldrich. All chemicals used in this study were of analytical grade and used as received without further purification. All solutions were prepared using twice distilled water.

2.2. Electrochemical and material measurements

Glassy carbon (GC, Metrohm, Herisau, Switzerland) of 3.0 mm in diameter electrode was used as working electrode after polishing with aqueous slurries of successively finer alumina powder on a microcloth. A spiral Pt wire and SCE were used as the counter and reference electrodes, respectively. Electrochemical measurements were performed at room temperature in a conventional three-electrode glass cell using a Galvanostat/Potentiostat Reference 3000 (Gamry Instruments). Electrochemical impedance spectroscopy (EIS) measurements were carried out at +0.44 V (N.B., Nyquist plot was first measured at different potentials and +0.44 V was selected as the best potential, at which the kinetic control region can be easily observed) with a disturbance potential of 5 mV and a frequency range from 1 MHz to 0.1 Hz. The equivalent circuit of Nyquist plots was simulated using the ZSimpWin software. A scanning electron microscope coupled with an energy dispersive X-ray spectrometer (SEM/EDS, HITACHI UHR FE-SEM SU8030) was used to evaluate the electrode morphology and composition. X-ray diffraction, transmission geometry XRD, (STOE STADI) operated with Cu K_α radiation (λ = 1.54 Å) and position sensitive detector was used to identify the change in the particle size and the crystallographic structure of the as prepared nickel-chitosan composites catalyst at different temperatures.

2.3. Chitosan-nickel oxyhydroxide nano-composites synthesis

Chitosan (CS) solution with a concentration of 1% (w/v) was prepared by dissolving 1 g of CS in 100 ml of 1% (v/v) acetic acid solution. The dissolution process took place at room temperature with stirring for 24 h. The obtained bright yellow solution was then filtered to remove various types of dust and impurities. In order to synthesize chitosan-nickel oxyhydroxide nanocomposites, 1 g of nickel sulfate was mixed with the above prepared CS solution under vigorous stirring for at least 3 h until almost transparent solution is obtained. The obtained chitosan-nickel solution was then titrated against 1 M sodium hydroxide under magnetic stirring until pH 10 to produce chitosan-nickel hydroxide microspheres in which nickel was *in-situ* formed inside the chitosan matrix during titration

with sodium hydroxide. The obtained CS-nickel hydroxide composite microspheres (average diameter was 0.65 mm) were kept under stirring for 5 h at room temperature and then filtered and washed with copious amounts of distilled water and ethanol to remove excess of nickel on the composite beds surface. Next, the obtained CS-nickel hydroxide beds were dried at 50 °C overnight. Consequently, the obtained CS-nickel oxyhydroxide catalyst was divided into six samples and heat treated at 160, 200, 230, 250, 280 and 300 °C for 3 h under nitrogen (Fig. S1 in Supporting information summarizes the catalyst preparation procedures). For the sample calcination, the oven temperature was adjusted and left until it reached the needed temperature and then the sample was introduced inside the oven and kept at this temperature for 3 h. The binding mechanism of nickel ions to chitosan matrix is not fully understood yet. However, previous literature [37–39] shows the binding of transition metal ions by chitosan is understood by coordination with the amino (—NH_2) and/or the hydroxy (—OH) groups on chitosan chains that serve as coordination sites. It is likely that the two —OH groups and the two —NH_2 groups are grabbed by one nickel and the chitosan-nickel complex is formed. The same above procedures but without adding nickel salt to the 1% (w/v) chitosan solution were used to synthesize chitosan beads. For the preparation of nickel hydroxide nanoparticles, 5.8 g of $NiSO_4$ was dissolved completely in 100 ml of deionized water. The nickel hydroxide nanoparticles were obtained via adding 1 M NaOH drop-by-drop to the $NiSO_4$ solution until pH ~10. The obtained green nickel hydroxide beads were then filtrated and dried at 50 °C for about 12 h and then calcined at 250 °C for 3 h. A suspension of chitosan-nickel nanocomposites, nickel hydroxide and chitosan to become anchored onto the GC electrode surface was prepared by adding the proper mass of the as-prepared catalyst powder in a test tube containing 1 ml isopropanol/water and one drop of Nafion solution (20% in water). The above mixture was ultra-sonicated for 5 h at room temperature (see Fig. S1-Supplementary information).

2.4. Electrode modification

Glassy carbon tip (GC), used here as the underlying substrate for chitosan-nickel oxyhydroxide nanocomposites, was mechanically polished using a polishing microcloth with aqueous slurries of 0.05 μm alumina powder and then rinsed thoroughly with distilled water and ethanol prior to modification. The modified electrode was prepared by the drop-coating procedure; 5 μl of a freshly prepared chitosan-nickel nanocomposites suspension (prepared as described above) was cast onto the cleaned GC surface and left to dry at 50 °C for about 20 min (see Fig. S1-Supplementary information). Casting different volumes on the GC electrode were used to prepare GC modified electrodes with different CS-nickel nanocomposites loading levels. In this manner, the GC electrode covered with chitosan matrix with uniformly dispersed and complexed nickel hydroxide was obtained. After that, the electrode was placed in the electrochemical cell with 0.1 M NaOH solution and potential was cycled between −0.2 and 0.63 V at a scan rate of 10 mV s^{-1} until a reproducible cyclic voltammogram is obtained, i.e., typically for 15 scans in order to convert metallic nickel (coordinated with CS) and nickel hydroxide to nickel oxyhydroxide. Subsequently the modified electrode was used in different experiments.

3. Results and discussion

3.1. Material and electrochemical characterizations

Fig. 1 illustrates the typical SEM images of CS (images A & B,), nano-NiOOH (images C & D) and nano-CS-NiOOH (images E & F) modified GC electrodes (*N.B.*, images A, C & E for the catalysts without any heat treatment, while images B, D & F for the annealed catalysts at 250 °C for 3 h before drop-casting onto GC surface). This figure reveals that CS modified GC electrode (CS/GC) has an irregular structure before heat treatment (Image A) and agglomerations of ill-hollow tube like structure after annealing at 250° (Image B). The heat treatment resulted in a significant change in the morphologies of nano-NiOOH and nano-CS-NiOOH modified GC electrodes as well. For instance, nano-NiOOH modified GC electrode (nano-NiOOH/GC) shows a big agglomeration of irregular particles before calcination (see Image C) and a nano-plate like structure with an average particle size of 63 nm after calcination (Image D), while nano-CS-NiOOH/GC electrode seems to form core-shell like structure homogenously covering the entire GC surface with an average particle size of 20 nm (Image E) before calcination and mixtures of nano-rod and nano-plate like structures with average particle size of 16 nm after calcination (Image F). Closer examination of images C and E shows that CS resulted in well-dispersed nanostructured nickel with smaller average particle size, while the heat treatment caused a significant change in the morphological structure and average particle size of the as-prepared catalysts, indicating the crucial role of using CS and heat treatment on the dispersion and morphology of nanostructured nickel. EDX was used to analyze the elemental composition of CS, nano-NiOOH and nano-CS-NiOOH modified GC electrodes (Insets of Fig. 1). Strong characteristic peaks of carbon, oxygen and nickel are observed for both nano-NiOOH/GC and nano-CS-NiOOH/GC electrodes, along with an additional weak peak for N which appeared in case of nano-CS-NiOOH/GC electrode, indicating the presence of chitosan on the GC surface. Carbon comes from both the substrate and chitosan. Oxygen species originated from the substrate, CS, and possibly oxide or hydroxide nickel species. The semi-quantitative results of each electrode are estimated by taking the average value of reading at three different spots on the electrode surface, data are listed as inset tables in Fig. 1. For instance, EDX revealed that nano-NiOOH/GC and nano-CS-NiOOH/GC electrodes have 51% and 30% nickel, respectively.

The crystallinity of the as-prepared catalysts was investigated using XRD, data are presented in Fig. 2. XRD patterns of CS/GC electrodes before (curve a) and after (curve a') calcination exhibited only one broad peak at $2\Theta = 20°$ attributed to C (002) and that may indicate the amorphous structure of CS. While nano-CS-NiOOH/GC electrode before (curve b) and after (curve b') calcination shows only the characteristic peaks of β-$Ni(OH)_2$ phase (JCPDS 00-014-0117) [40], nano-NiOOH/GC electrode (without heat treatment) reveals two nickel hydroxide phases (γ-$Ni(OH)_2$ and β-$Ni(OH)_2$, curve c). Those two phases are converted into a face-centered cubic (fcc) NiO crystalline structure after calcination (JCPDS, No. 04-0835, curve c') [40], indicating the essential role of CS in stabilizing the β-nickel hydroxide phase, which is well-known as the most active nickel phase even at high temperature. Scherrer equation was used to estimate the average crystallite size. The calculated average crystallite sizes of nano-NiOOH/GC electrode before and after calcination are 60 and 48 nm, respectively (N.B., the reflections around 33° (assigned for β-$Ni(OH)_2$) and 38° (assigned for NiO) were used to estimate the average particles size of nano-NiOOH/GC before and after heat treatment at 250 °C), and 25 and 19 nm for nano-CS-NiOOH/GC electrode before and after annealing using the diffraction peak of β-$Ni(OH)_2$ at ca. 33°, respectively. Additionally, XRD peak positions of nano-CS-NiOOH electrode are shifted slightly positive indicating the electronic interaction between nickel and chitosan.

Fig. 3 compares CVs of the bare GC and modified GC electrodes with CS, nano-NiOOH and nano-CS-NiOOH before (A) and after (B) calcination at 250 °C. As clearly seen in this figure, neither the bare GC (curve a) nor CS/GC (curve b) electrodes showed any features or peaks under measuring conditions, while a couple

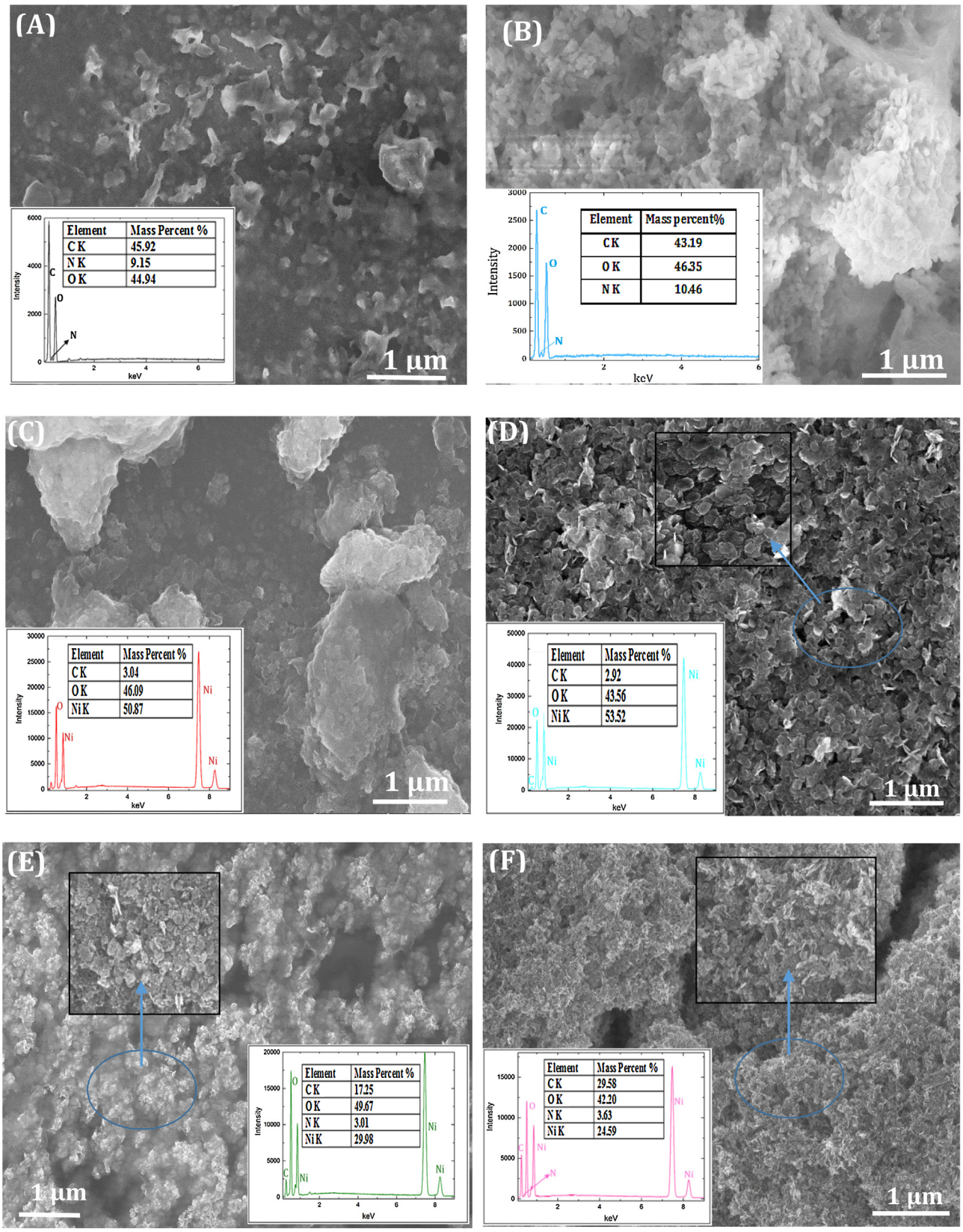

Fig. 1. SEM images and EDX analysis (inset of each image) for CS (A & B), nano-NiOOH (C & D) and nano-CS-NiOOH (E & F) modified GC electrodes before (A, C & E) and after (B, D and F) calcination at 250 °C for 3 h.

of well-defined redox peaks is observed for nano-NiOOH/GC electrode (curve c) with anodic peak at 0.52 V and cathodic peak at 0.21 V (potential separation of 0.31 V). It is worthy to mention here that the potential separation between anodic and cathodic peak is decreased to be 0.13 V and the intensity of those peaks is increased after calcination (curve cí). Previous research has attributed that

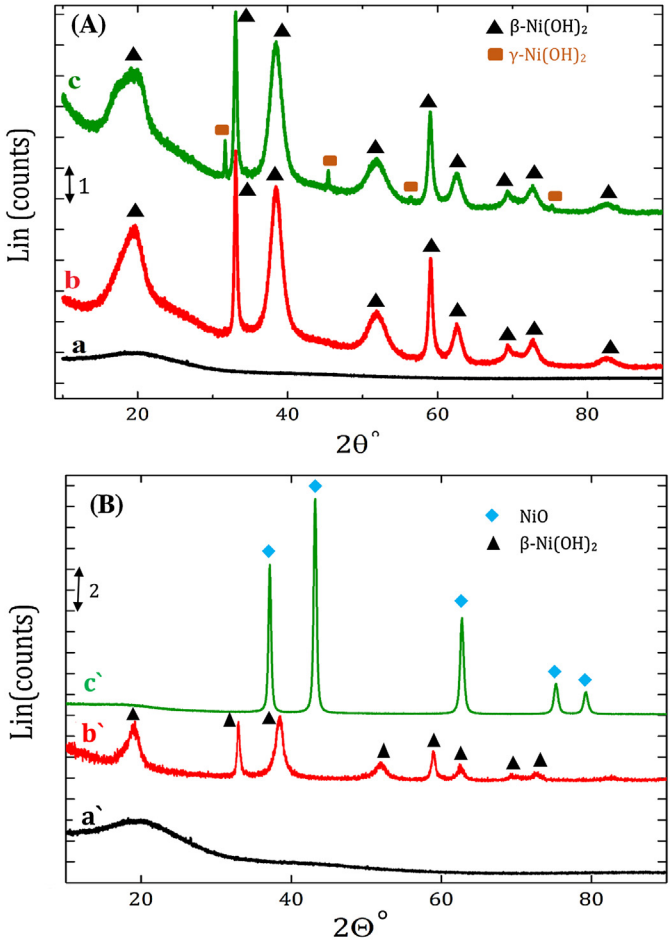

Fig. 2. XRD patterns obtained at CS (a & aí'), nano-CS-NiOOH (b & b') and nano-NiOOH (c & cí') modified GC electrodes before (A) and after annealing at 250 °C for 3 h (B). Note that a,b & c were assigned for the electrodes before calcination and aí, bí& cí were assigned for the same electrodes after calcination.

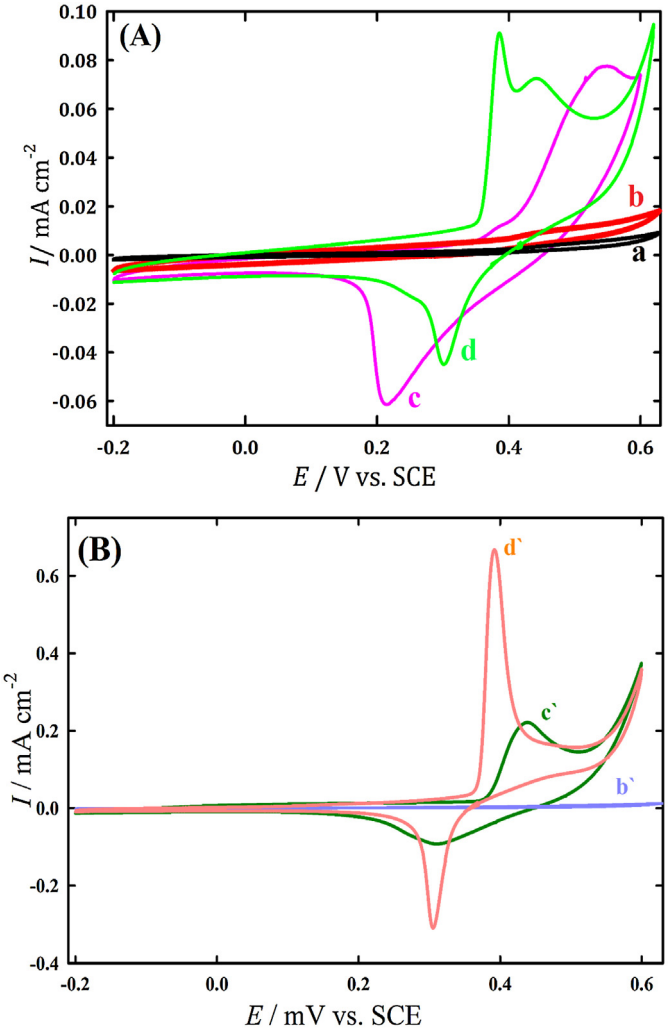

Fig. 3. CVs obtained at bare GC (a), CS/GC (b & bí), nano-NiOOH/GC (c & cí) and nano-CS-NiOOH/GC (d & dí) before (A) and after (B) calcination at 250 °C for 3 h in 0.1 N NaOH with scan rate of 10 mV s^{-1} (catalyst weight is 20 μg cm^{-2}). Note that curves b, c &d are used for the electrodes before calcination while curves bí, cí & dí are assigned for the same electrodes after calcination.

redox-peak couple to the surface confined $Ni(OH)_2$/NiOOH transformation [41]. Interestingly, nano-CS-NiOOH/GC electrode (before calcination, curve d) exhibited two oxidation peaks in the potential range of 0.38–0.54 V. The notable well-defined peak at 0.4 V might be resulting from the initial oxidation of metallic nickel (formed a coordination complex with CS matrix before NaOH treatment) to nickel hydroxide ($Ni(OH)_2$), and the peak around 0.45 V, which is slightly overlapped with the first peak, corresponds to the further oxidation of surface $Ni(OH)_2$ to nickel oxyhydroxide (NiOOH). Or one might attribute those two peaks to the various nickel hydroxide/oxyhydroxide transformations. It has been reported that nickel hydroxide based substrate has four possible phases, β-$Ni(OH)_2$, α-$Ni(OH)_2$, β-NiOOH, and γ-NiOOH, which are produced over the anodic and the cathodic scan. The transformations between these four phases can be well identified using the Bode diagram [35,36,41–44]. Significantly, this electrode exhibited only one sharp redox peak couple around 0.38 V with a low peak separation of 80 mV after calcination (curve d').

This might be attributed to the oxidation of all coordinated metallic nickel inside the CS matrix to nickel oxide species or the conversion of the less stable nickel hydroxide/oxyhydroxide phase to the more stable phase after calcination. We should mention here that XRD patterns did not detect any metallic nickel or change in the phase before and after calcination of nano-CS-NiOOH/GC electrode (see Fig. 2 (b &bí)). Thus one might safely argue that those two oxidation peaks may originate from the embedded β-$Ni(OH)_2$/NiOOH transformation inside that CS matrix and the surface β-$Ni(OH)_2$/NiOOH transformation. The average surface concentration of nickel, (Γ_{Ni}), was calculated to be 1.5 and 9.5 nmol cm^{-2} for nano-NiOOH/GC and nano-CS-NiOOH/GC electrodes before heat treatment, respectively, as estimated from the amount of charge consumed during $Ni(OH)_2$/NiOOH transformations (*i.e.*, Γ_{Ni} of nano-CS-NiOOH/GC electrode is 6 times higher compared with nano-NiOOH/GC electrode with the same nickel weight). This finding supports our assumption that CS helps in dispersing the nickel active phase on the GC surface via the formation of NiOOH with smaller particle size and thus preventing the coagulation of nickel nanoparticles. Additionally, calcination resulted in 5 and 3 times higher nickel active surface concentration for nano-CS-NiOOH/GC and nano-NiOOH/GC electrodes compared with the same electrodes before calcination, respectively.

3.2. Electrocatalytic activity

3.2.1. Glucose electrooxidation (Gox)

Fig. 4A shows the CVs of glucose electrooxidation (Gox) at bare GC and CS, nano-NiOOH and nano-CS-NiOOH modified GC electrodes in 0.1 NaOH containing 1 mM of glucose (the same

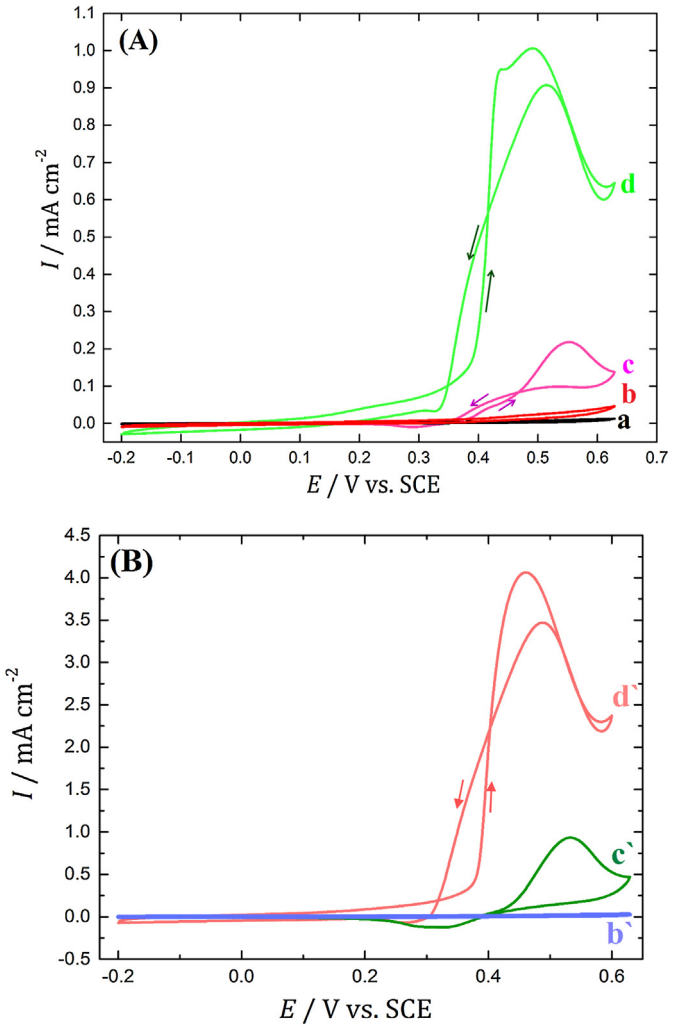

Fig. 4. CVs obtained at bare GC (a), CS/GC (b & bí), nano-NiOOH/GC (c & cí) and nano-CS-NiOOH/GC (d & dí) before (A) and after calcination at 250 °C (B) in 0.1 N NaOH containing 1 mM glucose with a scan rate of 10 mV s^{-1}. Note that curves b, c & d are assigned for the CVs before calcination and curves bí, cí & dí refer to the CVs after calcination. 20 μg cm^{-2} of catalyst were cast on GC surface.

electrodes, notations and colors are used as in Fig. 3). This figure revealed that the bare GC electrode has no electrocatalytic activity towards Gox (curve a), while CS/GC electrode (curve b) exhibited a poor electrocatalytic activity for Gox due to its large charging current. On contrast, the casting of nano-NiOOH (curve c) or nano-CS-NiOOH (curve d) onto the GC surface could significantly promote Gox, hence nickel nanoparticles are essential for higher rates of glucose oxidation. In the absence of glucose, both electrodes exhibited a pair of well-defined redox peaks corresponding to the $Ni(OH)_2$/NiOOH transformation (see Fig. 3). After adding glucose, a significant enhancement in the oxidative peak current associated with a significant decrease in the cathodic peak current occurred which resembles the behavior of a typical irreversible catalytic oxidation reaction. The mechanism of the glucose electrooxidation at nickel oxide modified electrodes is not a direct electron transfer from the sugar molecule to the anode, but occurs by a surface catalytic reaction between glucose and high-valence species of nickel. Note that the electrocatalytic oxidation of glucose occurs not only in the anodic scan but also in the cathodic direction. This phenomenon implies that the catalytically active sites are limited at high positive potentials, along with the accumulation of intermediates and reaction products on the electrode surface, thus resulting in the conclusion that glucose does not have enough time to undergo full oxidation in the forward anodic half cycle [37]. With the increase of the glucose concentration, the enhancement of the oxidative peak becomes more evident, and the cathodic peak ascribed to Ni(III) reduction gradually becomes unrecognizable (see Fig. S2).

Notably, nano-CS-NiOOH/GC electrode (Fig. 4A-curve d) exhibited 12 times higher electrocatalytic activity towards Gox (as calculated from the amount of charge associated with Gox) and approximately 0.15 V negative shift on the Gox onset potential compared with nano-NiOOH/GC electrode (Fig. 4A-curve c) with the same catalyst loading, indicating the essential role of CS in Gox enhancement. This enhancement might be attributed to the increase in the nickel oxyhydroxide active surface area. The size of nanostructured nickel in nano-CS-NiOOH/GC electrode is much lower than its size in absence of CS. The decrease in the size of nanostructured nickel was accompanied by an increase in its surface area and hence an increase in the peak current of Gox. It is worthy to mention that the surface area of nano-CS-NiOOH/GC electrode increased by a factor of 6, while its electrocatalytic activity improved by a factor of 12. Consequently, also other factors contributed in Gox enhancement in the presence of chitosan. A possible synergism between nanostructured nickel and the —OH and $—NH_2$ functional groups of chitosan may also be effective in Gox enhancement. The electrocatalytic oxidation of small organic molecules (e.g., methanol) and glucose is enhanced by the presence of —OH groups adsorbed on the GC surface [45–47]. Moreover, XRD patterns (Fig. 2) indicate that CS stabilizes the active NiOOH phase (β) rather than less active NiOOH phase (γ). Significantly, the heat treatment resulted in a further noteworthy improvement in Gox current of the both electrodes. For instance, heat treatment resulted in 3 and 6 times higher electrocatalytic activity of nano-NiOOH/GC and nano-CS-NiOOH/GC electrodes (comparing curves c & d with c‘ & d‘), respectively. This improvement might be attributed to the further decrease in the nickel particle size and/or the change in NiOOH morphology after calcinations as revealed from SEM images (see Fig. 1), besides the conversion of less active nickel hydroxide/oxyhydroxide phase to more active nickel phase as revealed from the appearance of only one oxidation peak in the forward scan direction after calcination in the presence (compare curves c &d of Fig. 4A with curves c‘& d‘ of Fig. 4B) and in the absence (compare curves c &d of Fig. 3A with curves c‘& d‘ of Fig. 3B) of glucose.

The Tafel slope estimated from the respective plots is 58 mV/dec for the nano-NiOOH/GC and nano-CS-NiOOH/GC electrodes (see Fig. S3), suggesting that the Gox mechanism does not change on the both electrodes and is a two-electron controlled process. Several Tafel slope values have been reported previously based on the electrode modifiers and the underlying substrate in the case of the same modifier. For instance, Tafel slopes for nickel oxide modified carbon nanotube and glassy carbon electrode equal to 167.5 and 128.3 mV $decade^{-1}$, respectively, have been reported [20,48]. A comparable value of 63 mV $decade^{-1}$ has been reported at Fe_2O_3 nanowire arrays [49].

EIS is a useful technique to study the electron transfer characteristics in the electrode–electrolyte interface and to track electrode surface modifications as presented in Nyquist complex-plane plots of differently-modified electrodes before heat treatment (Fig. 5A) and after calcination at 250 °C (Fig. 5B) in 0.1 N NaOH containing 1 mM glucose (Fig. 5). Two equivalent circuit models were used here to fit the experimental data; *model I* was used to fit the obtained data of bare and nano-NiOOH modified GC electrodes (Inset of Fig. 5A), while *model II* was used to fit CS and nano-CS-NiOOH modified GC electrodes data (Inset of Fig. 5B). The fitted values for each element are listed in Table S1. As expected, the bare GC electrode exhibits a very high resistance for both glucose oxidation and adsorption (i.e., no glucose molecule is adsorbed or oxidized on the bare GC surface, $R_{ct} = 1061\ \Omega$ and $R_{ads.} = 1.57 \times 10^5\ \Omega$, Fig. 5A-curve a). However, CS/GC elec-

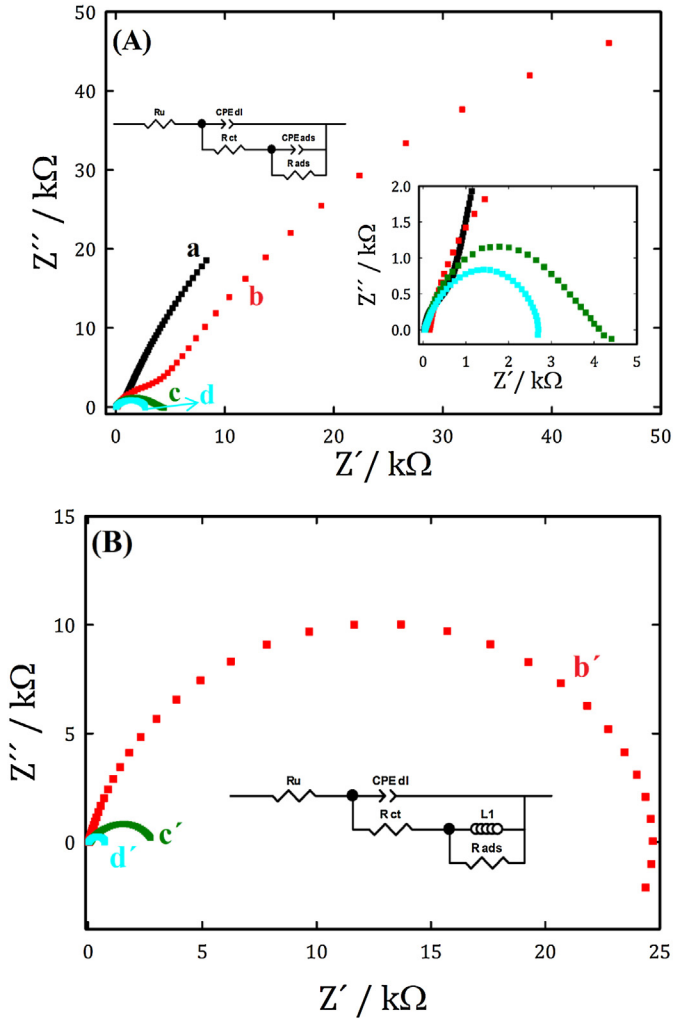

Fig. 5. Nyquist plot obtained at GC, CS/GC, $Ni(OH)_2$/GC and CS-$Ni(OH)_2$/GC at 0.44 V vs SCE in 0.1 N NaOH containing 1 mM glucose before (A) and after calcination at 250 °C (B). Note that curves b, c & d are assigned for the electrodes before calcination and curves bí, cí & dí refer to the electrodes after calcination. 20 μg cm^{-2} of catalyst were cast on GC surface.

trode resulted in a significant decrease in the glucose adsorption resistance which may be due to $-NH_2$ and $-OH$ like functional groups of CS helping glucose adsorption via hydrogen bond formation ($R_{ads.} = 3.54 \times 10^3$ Ω). The transfer resistance is significantly increased, which might be due to the interfacial electron transfer towards the electrode surface that is hindered by CS (R_{ct} = 5866 Ω, see Fig. 5A-curve b). Interestingly, modification of GC surface with nano-NiOOH resulted in a significant decrease in R_{ct} (731 Ω) and slight decrease in $R_{ads.}$ (4000 Ω), due to significantly improved electron transfer within nickel hydroxide/oxyhydroxide transformation (see Fig. 5A-curve c). On the other hand, R_{ct} (490 Ω) and R_{ads} (1991 Ω) of nano-CS-NiOOH/GC electrode further significantly decreased (see Fig. 5A-curve d), indicating the crucial role of NiOOH for the electron transfer and CS for glucose adsorption by providing favorable conduction pathways or probably by synergistic effects in the nanocomposites with chitosan functional groups. Therefore, nano-CS-NiOOH can dramatically improve both the electron transfer efficiency and adsorption step of glucose at the electrolyte–electrode surface compared with NiOOH and CS modified electrodes. Furthermore, the calcination of nano-NiOOH and nano-CS-NiOOH modified GC electrodes resulted in a further decrease in the charge transfer and adsorption resistance (compare curves b and c in Fig. 5A with curves bí and cí in Fig. 5B).

For instance, R_{ct} decreased to 230 and 300 Ω for calcined nano-CS-NiOOH/GC and nano-NiOOH/GC electrodes, respectively, and R_{ads} is reduced to 2155 and 431 Ω for nano-CS-NiOOH/GC and nano-NiOOH/GC electrodes, respectively. This indicates the vital role of the heat treatment step in conversion of the less active nickel oxide phase to the highly active one.

The effect of nanostructured nickel loading towards the electrocatalytic oxidation of glucose has been investigated. As mentioned above, the existence of nickel nanoparticles and the $Ni(OH)_2$/NiOOH transformation redox-couple is essential for the electrocatalytic oxidation of glucose; so already small loadings of the nickel nanoparticles at the GC result in a significant enhancement of the electrocatalytic activity of the GC toward Gox. Fig. 6A shows the CVs obtained at nano-CS-NiOOH/GC electrode with different loadings in 0.1 N NaOH. As revealed from this figure, the $Ni(OH)_2$/NiOOH redox peak couple around 0.4 V is increased as the loading of nickel is increased. The surface concentration of nickel oxide species (Γ_{Nickel}) was estimated by integrating the area under the anodic peak of the $Ni(OH)_2$/NiOOH redox couple at different loadings using the following equation [50]:

$$\Gamma_{Nickel} = \frac{Q}{nF} \quad (4)$$

where Q is the charge density in coulombs/cm^2, n is the number of the electrons involved in the reaction (n = 1 according to Eqs. (1) and (2) and F is Faradayís constant. As clearly seen in Fig. 6A (inset a), the surface concentration of nickel oxide species is increased with increasing nickel nanoparticles weight and the nickel surface concentration of nano-CS-NiOOH/GC electrode (red-line) is ca. 5-fold higher compared with nano-NiOOH/GC (black-line) electrode with the same nickel weight. We may conclude that in spite of the equal nickel nanoparticles loading, the concentration of electrochemically active species of nano-CS-NiOOH/GC is 5 times higher, *i.e.*, CS resulted in the formation of smaller well-dispersed particles of nickel oxide species, that may result in an increased number of edges, corners and defects. The calculated values of Γ were used to estimate the loading of NiOOH of nano-NiOOH/GC and nano-CS-NiOOH/GC electrodes using the following relation; (NiOOH estimated loading = Γ * Molar mass of NiOOH * 1000), and then used to calculate the utilization percentage of NiOOH (UP%) as following:

$$UP\% = (^{EstimatedLoading}/_{ActualLoading}) \times 100 \quad (5)$$

NiOOH average utilization percentage for nano-CS-NiOOH/GC is around 45%, while it is only 4% for nano-NiOOH/GC electrode (Fig. 6A (inset b)). That is to say, catalyst utilization of nano-CS-NiOOH/GC electrode is 10 times higher compared with nano-NiOOH/GC electrode which points out the essential role of CS for nickel oxide active species dispersion on the surface.

Fig. 6B shows the LSVs of nano-CS-NiOOH/GC with different loadings in 0.1 N NaOH solution containing 1 mM glucose. As seen in this figure, as the loading of nanostructured nickel increases, the peak current of glucose oxidation increases and the onset potential shifts to lower positive values. Inset of this figure shows the variation of the amount of charge associated with glucose electrooxidation (Q_{Gox}) at nano-CS-NiOOH/GC electrode with the nickel loading. As revealed from this figure the Q_{Gox} linearly increases with increase in nickel weight, until a nickel weight of 20 μg cm^{-2}. Beyond this value further increase resulted in a slight increase on the catalytic activity of nano-CS-NiOOH/GC electrode (i.e., any further nickel after this value will belong to the bulk and is not involved in Gox). Fig. 6C shows the Nyquist plot obtained at the same electrode with different loadings at 0.44 V. As clearly seen from this figure, the charge transfer resistance systematically decreased with the nickel loading.

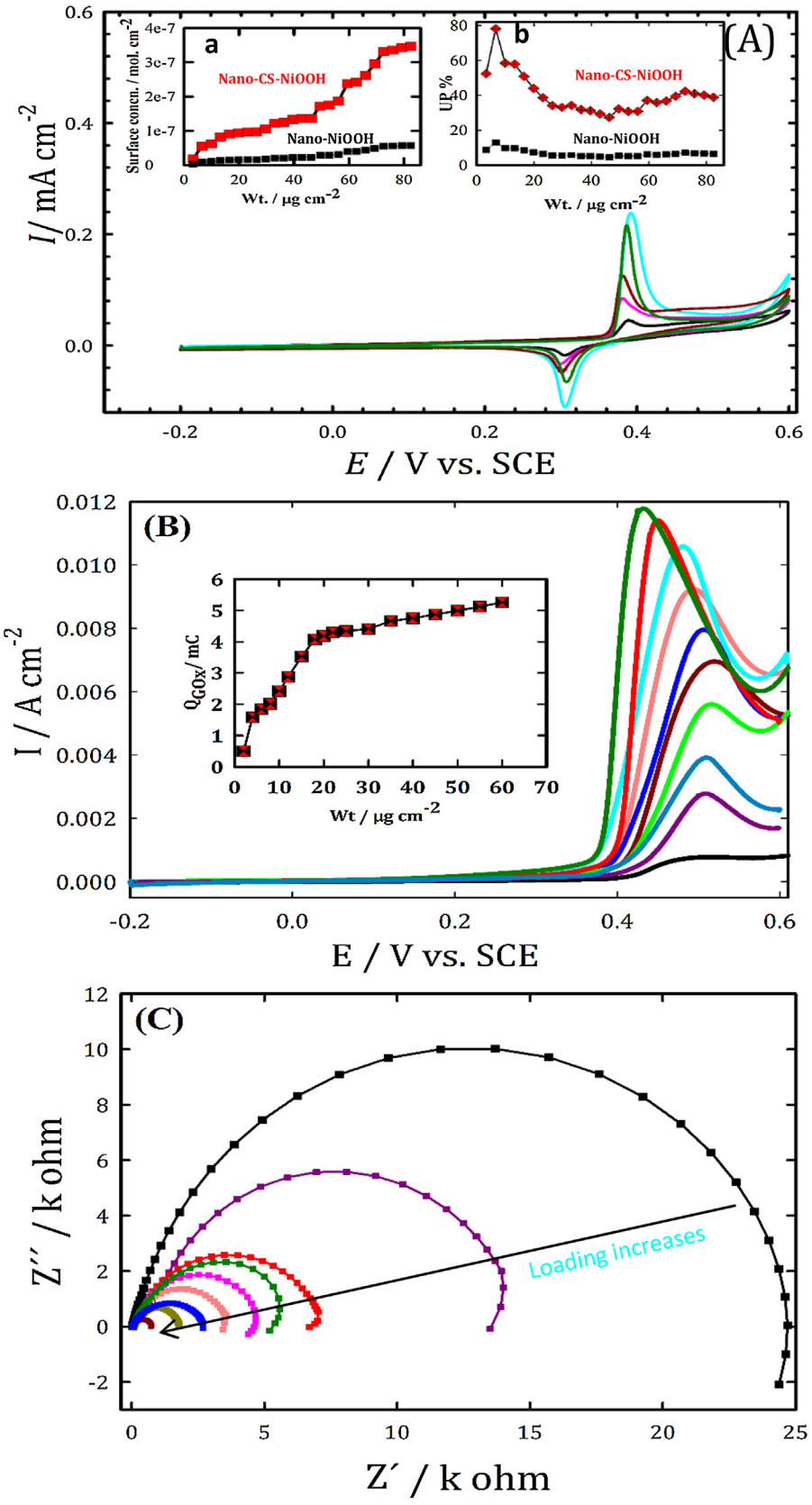

Fig. 6. (A) CVs of nano-CS-NiOOH/GC electrode with different NiOOH loadings (typically; 2, 10, 20, 30 and 50 μg/cm^2) in 0.1 N NaOH with a scan rate of 10 mV s^{-1} (insets show the variation of nickel surface concentration and catalyst utilization with nickel weight). (B) LSVs of glucose oxidation (1 mM) obtained at CS-NiOOH/GC electrode with different NiOOH loadings with a scan rate of 10 mV s^{-1} (inset shows the variation of the amount of charge associated with glucose oxidation with nickel weight) and (C) Nyquist plot obtained at the same electrode with different loadings (minimum loading is 2 μg/cm^2 and maximum loading is 50 μg/cm^2) at +0.44 V in 1 mM glucose solution.

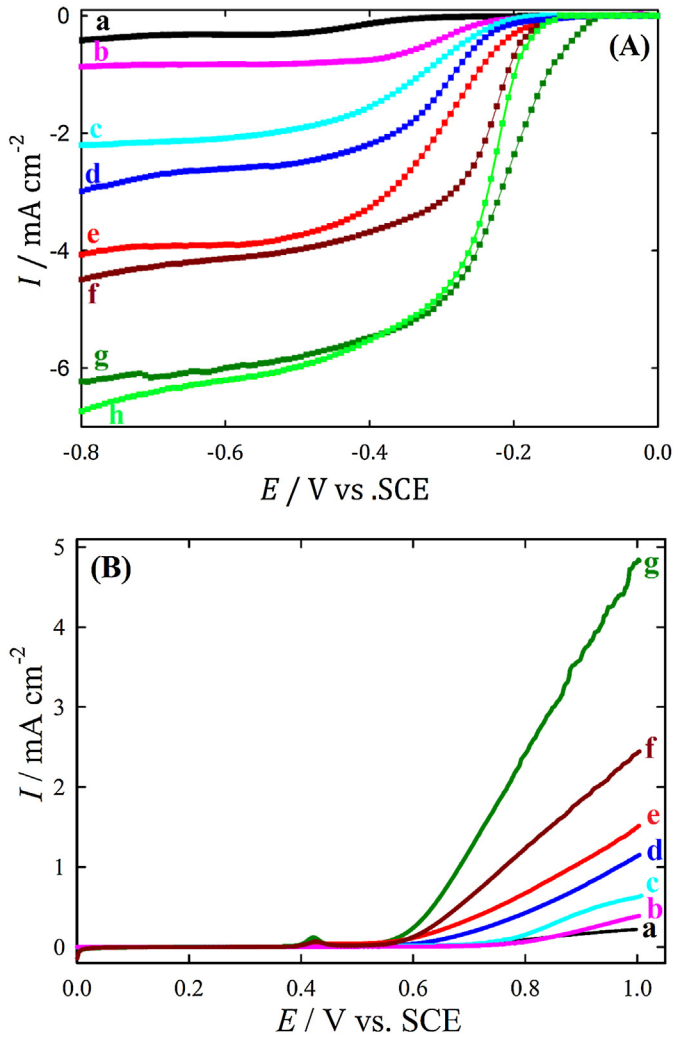

Fig. 7. (A) LSVs obtained in O_2 saturated 0.1 N NaOH at bare GC (a), CS/GC (b & c), nano-NiOOH/GC (d & e), nano-CS-NiOOH/GC (f & g) and Pt/C (h) with a rotation rate of 1600 rpm. Catalyst loading was 0.14 mg cm^{-2} for all Pt-free electrodes and 60 μg cm^{-2} for Pt/C electrode. Curves c, e and g show the calcined electrodes at 250 °C. (B) LSVs in 0.1 N NaOH at the same electrodes with a scan rate of 10 mV s^{-1} (same notations and colors were used as in A).

3.2.2. Oxygen reduction and evolution reactions (ORR & OER)

To assess the catalytic activity of as-prepared catalysts for ORR, LSV measurements were carried out on a RDE set up for bare GC, CS, nano-NiOOH, nano-CS-NiOOH and Pt (E-TEK) modified GC electrode before and after heat treatment at 250 °C in 0.1 N NaOH at a rotation rate of 1600 rpm (see Fig. 7A). As shown in Fig. 7A, the bare GC electrode (curve a) has a sluggish ORR activity as evident by the low onset potential (~−0.37 V) and the fact that it is a two-step two-electron reduction reaction of O_2 to OHH^-. CS/GC electrode (curve b) showed a more positive onset potential (~−0.25 V) and a higher diffusion limiting current density compared with the bare GC electrode, indicating the importance of the CS in enhancing the ORR activity. Additionally, annealing of CS/GC electrode resulted in a further ORR activity enhancement as indicated by higher onset potential (~−0.20 V) and one-step four-electron process (see curve c). As expected nano-NiOOH/GC electrode without heat treatment (curve d, with onset potential of ~−0.19 V) and after calcination at 250 °C (curve e, with onset potential of ~−0.16 V) exhibited a higher electrocatalytic activity for ORR compared with both bare GC and CS/GC electrodes. Surprisingly, the ORR activities obtained at nano-CS-NiOOH/GC electrode before (curve f) and after calcination (curve g) are greatly enhanced. This might be due to the synergistic effect between nano-NiOOH and CS. For instance, calcined nano-CS-NiOOH/GC electrode (curve g) exhibited an ORR half-wave potential ($E_{1/2}$) of ca., −0.17 V (~48 mV more positive compared with Pt/C) and onset potential of ca. 0.01 V (~40 mV more positive than that of Pt/C), which is slightly better than the commercial Pt/C (E-TEK) electrode (curve h). This strongly suggests that nano-CS-NiOOH/GC electrode is an efficient electrocatalyst for ORR with higher electrocatalytic activity than Pt/C with 20 wt% Pt. It is worthy to mention here that the electrocatalytic activity of nano-CS-NiOOH/GC electrode for ORR increases as the loading of NiOOH increases, as indicated by the linear positive shift on the $E_{1/2}$ and onset potential with increasing loading (See Fig. S4A).

Kinetic data in terms of Tafel slopes were estimated using the data of Fig. 7A (Fig. S5 A). In the perspective of achieving high current at low overpotential, a lower slope becomes an indicator of a better catalytic performance [51]. Tafel slopes of 63, 73, 100, 119 and 136 mV/decade were measured for nano-CS-NiOOH/GC, Pt/C, nano-NiOOH/GC, CS/GC and GC electrodes, respectively, indicating the higher activity of nano-CS-NiOOH/GC electrode compared to the other studied electrodes.

In order to investigate the electrocatalytic activity of nano-CS-NiOOH/GC and nano-NiOOH/GC (un-calcined and calcined) electrodes for OER, their LSVs in 0.1 N NaOH at a scan rate of 10 mV s^{-1} were measured (data presented in Fig. 7B). As clearly seen from this figure, un-calcined (curve b) and calcined CS/GC electrodes (curve c) exhibited a better electrocatalytic activity compared with the bare GC electrode (curve a). Expectedly, the calcined (curve d) and un-calcined (curve e) nano-NiOOH/GC electrodes provided a higher OER activity compared with both bare GC and CS/GC electrodes, indicating the essential role of NiOOH in catalyzing OER. Interestingly, nano-CS-NiOOH/GC electrode before (curve f) and after annealing at 250 °C (curve g) showed an abrupt increase in OER current and a significant negative shift in OER onset potential, suggesting higher electrocatalytic activity of nano-CS-NiOOH/GC electrodes for OER. For instance, the onset potential of calcined nano-CS-NiOOH/GC electrode is 0.47 V vs. SCE, which is 0.37, 0.32, 0.30, 0.17and 0.13 V less positive than that of the bare GC, CS/GC, calcined CS/GC, nano-NiOOH/GC and calcined nano-NiOOH/GC electrodes, respectively, demonstrating the higher electrocatalytic activity of nano-CS-NiOOH/GC electrode for OER than the other catalysts. Furthermore, the OER activity of CS-NiOOH/GC electrode increased as the loading of NiOOH increased (See Fig. S3B). Tafel slopes of 197, 176, 142 and 79 mV/decade were obtained for GC, CS/GC, nano-NiOOH/GC and nano-CS-NiOOH/GC electrodes, respectively (Fig. S5 B). A plausible explanation for the higher electrocatalytic activity of the nano-CS-NiOOH modified electrode for OER is that CS resulted in a higher active surface area and also enhanced the adsorption of oxygen active species using its functional groups. In addition to that, CS resulted in a significant decrease in the size of the formed gas bubbles (i.e., oxygen bubbles, which stay in contact with the catalyst until they get detached from the electrode surface). This helps to increase bubble detachment from the electrode surface and lowers the time, the catalyst is in contact with oxygen, thus resulting in a stable active nickel oxide phase for longer times (see Fig. S6).

3.3. Effect of calcination temperature

Generally, metal oxides are synthesized at different calcination temperatures and it has been previously reported that the calcination temperature has a dramatic effect on the specific surface area and the particle size of the prepared metal oxide catalyst [52–55]. Structural modifications, such as changes in surface geometry (clusters, crystal planes, adatomes), and differences in the electronic state of the catalyst material were observed. From the

above results, the heat treatment resulted in a significant increase of the electrocatalytic activity of the as-prepared catalysts. This finding motivated us to investigate the heat treatment effect on the catalysts activity and morphology (*i.e.*, investigate the origin of enhancement). SEM images of nano-CS-NiOOH/GC electrode reveal a significant change of the nano-CS-NiOOH morphology and average particle size with the increase in calcination temperature (see Fig. S5). For instance, nano-CS-NiOOH before heat treatment showed a core-shell like structure, whereas NiOOH forms "worm-like structures" incorporated inside the CS matrix, with average particle size of 20 nm, while it exhibited nano-rods (with average particle size of 15 nm) and a mixture of nano-rods and nano-plates (average particle size is 10 nm) after calcination at 200 and 250 °C, respectively. Specifically, for calcination temperatures higher than 280 °C nano-CS-NiOOH is formed in the irregular shape of big agglomerates. This may be attributed to the destruction of the CS matrix at this temperature (TGA and SEM of CS at various temperatures indicated that CS matrix starts to degrade above a temperature of 280 °C, data not shown [56]), pointing out the essential role of CS matrix in avoiding the aggregation of nickel nanoparticles and its vital role in improving NiOOH surface dispersion. Moreover, EDX analysis of nano-CS-NiOOH/GC showed a peak for nitrogen which belongs to CS structure before 280 °C and there is no nitrogen peak observed above this temperature. That may be used as evidence for the destruction of CS matrix after this temperature as well (see inset of Fig. S7).

Fig. 8 (A&B) shows the CVs measured at nano-CS-NiOOH/GC electrode at various annealing temperatures in 0. 1 N NaOH solution with a scan rate of 10 mV s^{-1}. This figure depicts that the current density of the $Ni(OH)_2$/NiOOH transformation is increased with increasing calcination temperature and reached its maximum value at 270 °C (Fig. 8A (a–d)). Interestingly, beyond this temperature the current density of $Ni(OH)_2$/NiOOH dropped down significantly (Fig. 8B (e–h)). This may be due to the coalescence of the nickel nanoparticles after the destruction of the CS matrix as indicated from the SEM images which resulted in a significant decrease in the surface area (Fig. S7). While only one oxidation peak around 0.4 V is observed for the calcination temperature ≤280 °C and most likely belongs to the β/β-$Ni(OH)_2$/NiOOH transformation as evident from XRD pattern, (c.f Fig. 8C), two oxidation peaks around 0.4 and 0.5 V are detected at calcination temperatures of 320 °C. Those two peaks may be attributed to β/β- and α/γ- $Ni(OH)_2$/NiOOH transformations. In other words, the amount of β-nickel oxyhydroxide increases with an increase of calcination temperature from 160 to 280 °C (curves a–d). After this temperature, β-nickel oxyhydroxide phase is converted to the less active γ- nickel oxyhydroxide phase as indicated from the decrease in the peak at 0.4 V and the appearance of a new peak at 0.5 V (curves e–h). This finding again emphasizes our assumption that CS matrix stabilizes the active nickel phase and prevents its coagulation. Inset of Fig. 8A revealed that the surface concentration of nickel oxyhydroxide for the nano-CS-NiOOH/GC electrode increases with the calcination temperature increase and reaches its maximum value at 280 °C. Then it significantly decreases beyond this temperature due to the aggregation of nickel nanoparticles after the destruction of CS membrane matrix. On the other hand, the surface concentration of nano-NiOOH/GC electrode continuously increases with the calcination temperature. XRD patterns were measured to investigate the change of the nanostructured nickel phase of nano-CS-NiOOH/GC electrodes with the annealing temperatures (data are presented in Fig. 8C). XRD patterns revealed that there is no change in the nanostructured nickel phase for annealing temperatures ≤280 °C (curves a–c; only the typical diffraction peaks of β-$Ni(OH)_2$ were observed).

Interestingly, XRD patterns of the annealed samples at 280 °C (at this temperature CS structure starts to degrade) show the beginning of the formation of the γ-$Ni(OH)_2$ phase (curve d) which is converted into NiO phase with further increase in the annealing temperature (curves e–f). This again supports our assumption that CS is important for stabilizing the nanostructured β-nickel phase. Fig. 9A & B (note that same notations and colors are used as in Fig. 8 A & B) shows LSVs of Gox at nano-CS-NiOOH/GC electrodes treated at different calcination temperatures. As can be seen in this figure, the electrocatalytic activities of the measured electrodes towards Gox are totally in agreement with the CVs measured in absence of glucose (Fig. 8 A & B). The glucose oxidation peak current is increased with the annealing temperature and reached its maximum value at 270 °C due to the increase in the β-NiOOH sur-

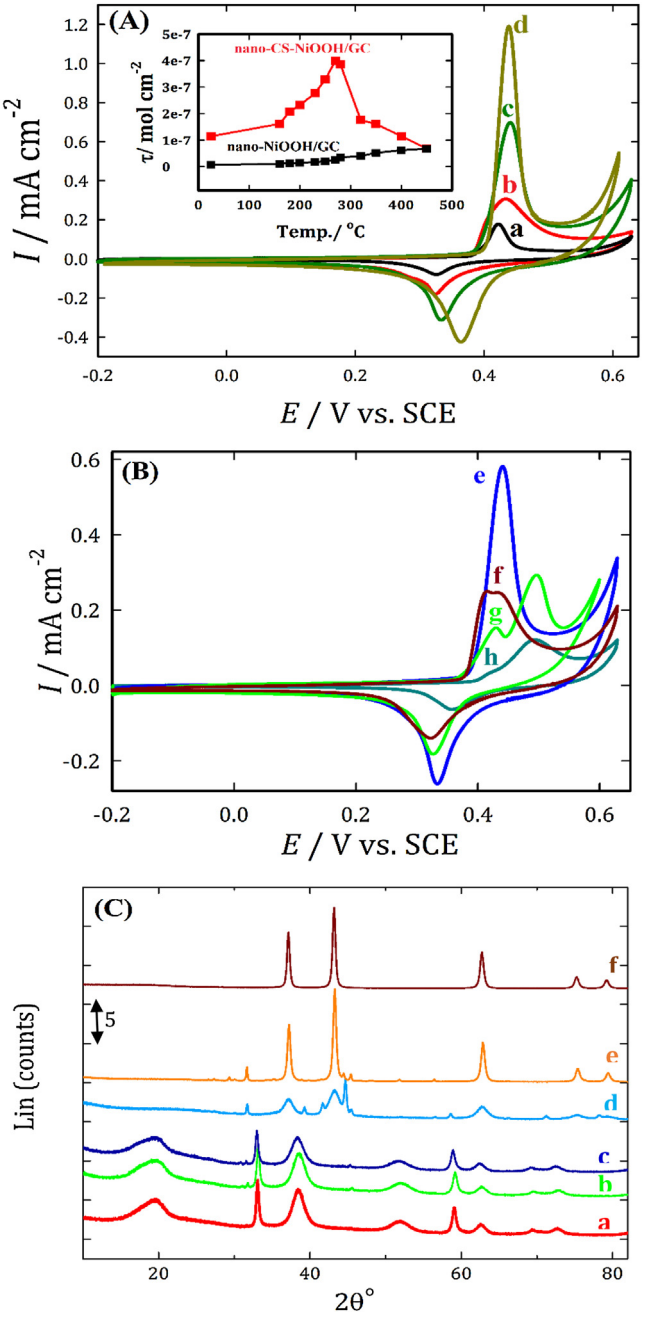

Fig. 8. (A&B) CVs of the nano-CS-NiOOH/GC electrode annealed at different temperatures (a) 180, (b) 200, (c) 250, (d) 270, (e) 280, (f) 300, (g) 350 and (h) 400 °C in 0.1 N NaOH with a scan rate of 10 mV s^{-1}. Inset shows the variation of NiOOH surface concentration of nano-NiOOH/GC and nano-CS-NiOOH/GC electrodes with the annealing temperature. (C) XRD of nano-CS-NiOOH/GC electrode at various annealing temperatures; typically, (a) 180, (b) 200, (c) 250, (d) 280, (e) 300, (f) 320 and (g) 450 °C.

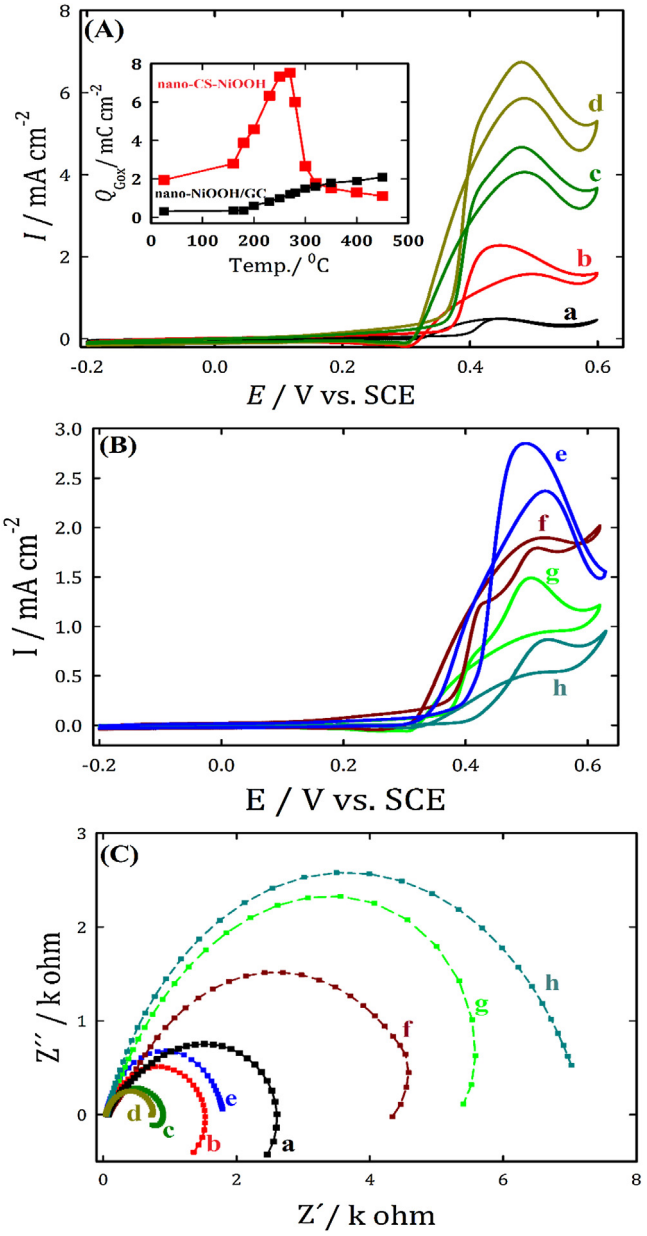

Fig. 9. (A&B) LSVs of glucose oxidation (1 mM) at nano-CS-NiOOH/GC electrode treated at various annealing temperatures, typically; (a) 180, b) 200 °C, c) 250 °C,(d) 270 °C, (e) 280 °C, (f) 300 °C, (g) 350 °C and (h) 400 °C with scan rate of 10 mV s^{-1}. (C) Nyquist plot of same electrodes measured at 0.44 V.

face concentration (see Fig. 9A (a–d) & inset of Fig. 9A). Beyond this temperature the glucose oxidation current decreased significantly due to the aggregation of NiOOH nanoparticles and the conversion of highly active β-phase to less active γ-phase, which resulted from the destruction of CS matrix above this temperature (Fig. 9B (e–h) & inset of Fig. 9A). Additionally, two glucose oxidation peaks (at 0.43 and 0.52 V) are observed for the calcined electrode at 300 (curve f) and 350 (curve g) °C which are attributed to Gox mediated at two different nanostructured nickel phases (most likely, α/γ and β/β- $Ni(OH)_2$/NiOOH transformations). Those two peaks are converted into only one oxidation peak at 0.53 V at a calcination temperature of 450 °C (curve h) and this indicates the essential role of CS in stabilizing the active nickel oxyhydroxide phase. Inset of Fig. 9A shows the variation of the amount of charge associated with glucose oxidation (Q_{Gox}) at nano-NiOOH/GC and nano-CS-NiOOH/GC electrodes with the annealing temperature. While the Q_{Gox} of nano-CS-NiOOH/GC electrode increases and reaches its maximum at a calcination temperature of ≤280 °C and significantly decreases above this temperature, the Q_{Gox} of nano-NiOOH/GC electrode continuously increases with the increase of annealing temperature. It is worthy to mention that the electrocatalytic activity of nano-CS-NiOOH/GC electrode for Gox is ca. 8 times higher at any temperature below 280 °C. The plausible explanation for this observation is that CS enhanced the glucose oxidation via stabilizing NiOOH active phase and increasing its surface concentration and additionally enhanced glucose adsorption via its functional groups. EIS measurements of nano-CS-NiOOH/GC electrode at various calcination temperatures revealed that Gox charge transfer resistance decreased with the annealing temperature and reached its minimum value at 270 °C, see Fig. 9C (a–d, solid-lines), and it significantly increased again beyond this temperature (see Fig. 9B (e–h, dotted-lines)). That again indicates the essential role of CS matrix on enhancing the Gox via an increase in surface concentration and stabilization of the β-nickel oxyhydroxide, as well as enhanced glucose adsorption via its —OH and —NH_2 functional groups.

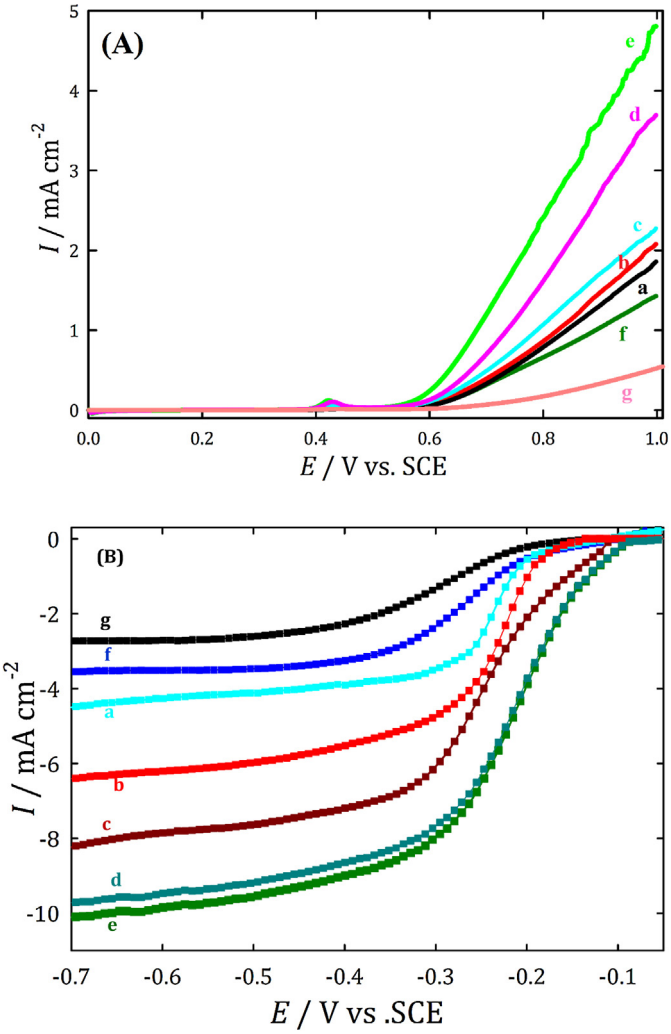

Fig. 10. (A) OER measured in 0.1 N NaOH solution and (B) ORR measured in O_2-saturated 0.1 N NaOH solution at nano-CS-NiOOH/GC electrode calcined at various temperatures, typically; (a) without heat treatment, (b) 180, (c) 200, (d) 250, (e) 280, (f) 300 and g) 350 °C.

Furthermore, the electrocatalytic activity of nano-CS-NiOOH/GC electrode towards ORR (Fig. 10A) and OER (Fig. 10B) exhibited the same behavior of glucose electrooxidation at the same elec-

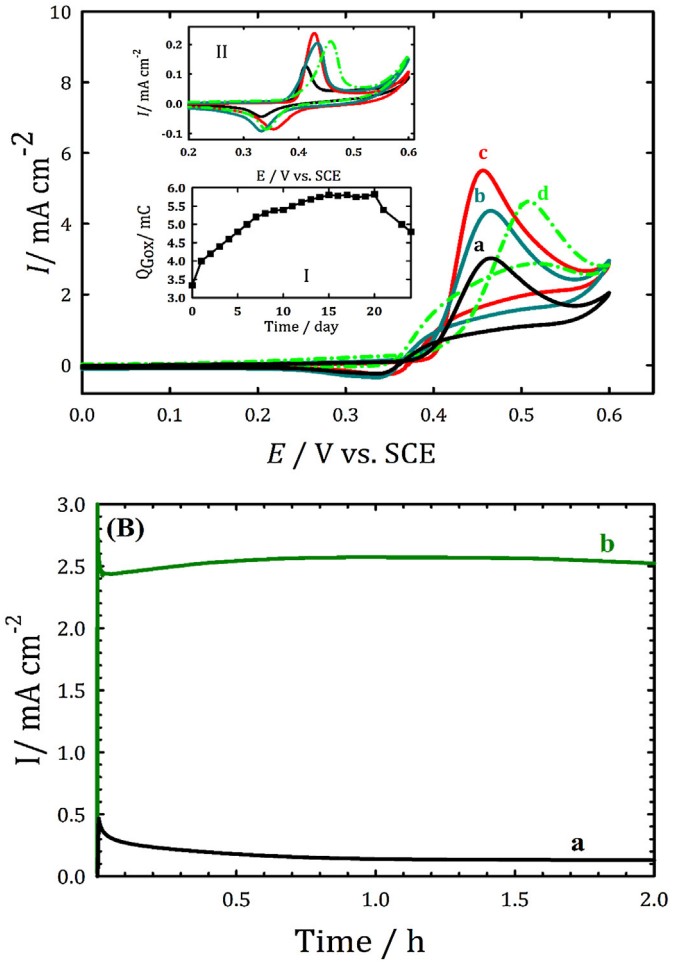

Fig. 11. (A) CVs of Gox at nano-CS-NiOOH/GC before (a) and after ageing for (b) one week, (c) two weeks and (d) three weeks in 0.1 N NaOH with scan rate of 10 mV s^{-1} (insets show (I) the variation of Gox peak current intensity with ageing time and (II) CVs of the same electrode at various ageing times). (B) *i–t* curve measured at (a) nano-NiOOH/GC and (b) nano-CS-NiOOH/GC electrodes at 0.44 V.

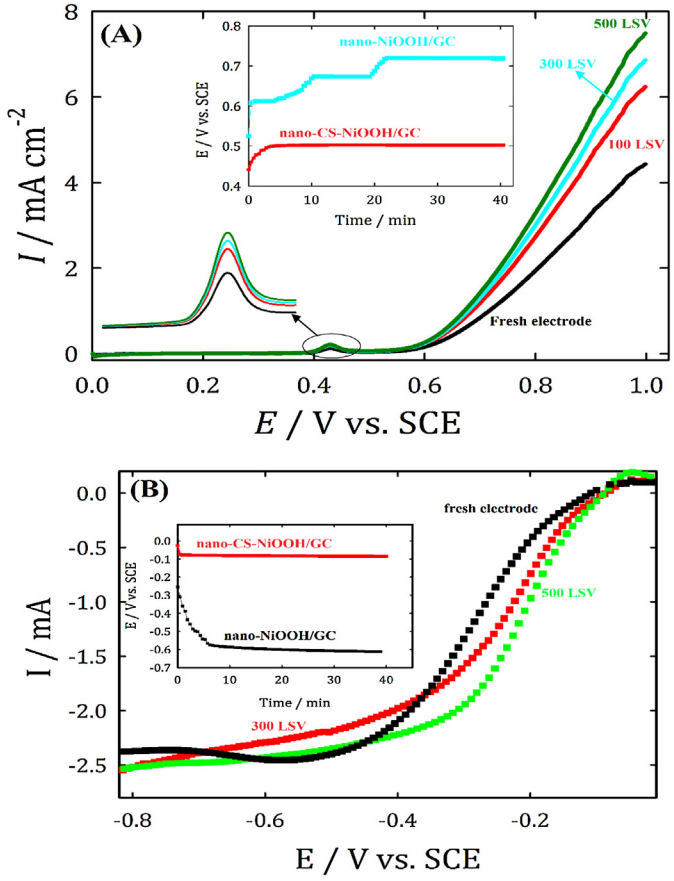

Fig. 12. Successive LSVs of (A) OER and (B) ORR at nano-CS-NiOOH/GC electrode in 0.1 N O_2-saturated NaOH with scan rate of 5 mV s^{-1}. Inset of each figure shows the E–t curve obtained at 1 mA cm^{-2}.

trodes, whereas the electrocatalytic activity of nano-CS-NiOOH/GC electrode towards OER and ORR is increased with the increase of calcination temperature (≤280 °C, see curves a–e in Fig. 10) and significantly decreased above this temperature (>280 °C). This might be explained by the conversion of nickel active phase (β-NiOOH) to less active phase (γ-NiOOH or NiO) due to the CS matrix destruction at calcination temperatures above 280 °C.

3.4. Stability and ageing effects

Fig. 11A shows CVs of Gox obtained at nano-CS-NiOOH/GC electrode before (a) and after ageing for various times (curves b–d) in 0.1 N NaOH containing 1 mM glucose with a scan rate of 10 mV s^{-1}. As clearly seen in this figure, the electrocatalytic activity of nano-CS-NiOOH/GC electrode for Gox is increased with ageing time and reached its maximum value after 21 days (curves a–c & inset I). After this time its activity significantly decreased and Gox peak shifted to more positive potentials (curve d and inset I). To explain this observation CVs of the same electrode were measured in absence of glucose (see inset II, same colors are used as in Fig. 11A). As revealed from this figure (inset II), the surface concentration of NiOOH systematically increased with ageing time (solid-lines) and after 21 days of continuous ageing the intensity of nickel hydroxide/oxyhydroxide transformation is significantly decreased and shifted to higher positive potentials (dotted-green line). This may be attributed to the formation of less active γ-NiOOH phase and might explain why the electrocatalytic activity of Gox was reduced after 21 days. Moreover, the stability of nano-CS-NiOOH/GC electrode was also investigated using chronoamperometry (see Fig. 11B). As clearly seen from this figure, nano-CS-NiOOH/GC electrode supports a higher Gox current (approximately 10 times higher) and stability compared with nano-NiOOH/GC electrode with the same nickel loading. For instance, the electrocatalytic activity of nano-NiOOH/GC electrode is reduced by 70% after one hour of continuous Gox at 0.44 V (Fig. 11B- curve a), while the activity of the nano-CS-NiOOH/GC electrode remains unchanged.

Fig. 12A shows successive LSVs (typically; LSVs number 1, 200, 300 and 500) of nano-CS-NiOOH/GC electrode in 0.1 N NaOH with a scan rate of 5 mV s^{-1}. It demonstrates that the electrocatalytic activity of nano-CS-NiOOH/GC electrode is improved, as the number of LSVs increased. For instance, after 500 LSVs a significant enhancement in catalytic activity towards OER is observed. That is, a 137 mV negative shift was obtained at a current density of 1 mA cm^{-2}. This behavior might be explained in view of the increase in the amount of β-NiOOH with ageing, which is the most active nickel phase for OER. The increase in the β-NiOOH could be revealed by calculating the active charge, Q, associated with the $Ni(OH)_2$/NiOOH transformation (The values of Q after various ageing times were calculated by integrating the area under the anodic peak observed at ca. 0.43 V, see zoom area in Fig. 12A). For the fresh electrode its value was 0.52 mC cm^{-2}, whereas its value increased to 2.3 mC cm^{-2} (four times higher) for the aged electrode for 500 LSVs in alkaline medium. Thus, it would appear that the current density for the OER at a particular overpotential is proportional to

the amount of active nickel oxide material. This effect was noted by Chialvo et al. who concluded that for nickel oxides of the same type (i.e. α-$Ni(OH)_2$ or β-$Ni(OH)_2$), this effect should be related to increasing surface roughness associated with the increasing amount of active material. Furthermore, inset of Fig. 12A shows the *E-t* (chronopotentiometry) curve obtained at nano-NiOOH/GC and nano-CS-NiOOH/GC electrodes at a current density of 1 mA cm^{-2}. This figure depicts that nano-CS-NiOOH/GC electrode has a higher electrocatalytic activity towards OER and stability compared with nano-NiOOH/GC electrode with the same weight.

In contrast, the OER onset potential of nano-CS-NiOOH/GC electrode remains constant at 0.5 V, while the onset potential of nano-NiOOH/GC electrode shifted to a higher positive potential with time. To explain this behavior, we imaged the bubble formation processes that happened on the electrode surface during *E-t* measurement. For the nano-NiOOH/GC electrode, after 5 min' bubbles start to accumulate on the electrode surface instead of dislodging from it (rate of bubble accumulation is faster than its rate of dislodging). This might be explained by the two-step positive shift of the *E-t* curve of this electrode (each step refers to bubbles accumulation and dislodging), while nano-CS-NiOOH/GC electrode has a smaller bubble size and a higher rate for bubbles detachment from the electrode surface compared with nano-NiOOH/GC electrode. Bubble size and rate of detachment of bubbles from the electrode surface were found to have a significant effect on the electrode performance (i.e., efficiency, stability and durability) towards OER. As the bubble accumulation rate and size increase, the electrocatalytic activity of the catalyst decreases. This may be explained by bubbles accumulation, which results in poisoning of the electrode surface area via a decrease in the available electroactive surface area and/or deactivation of the nickel oxide active phase via oxidation of the active phase to the less active phase (in our case, it may be oxidized β-NiOOH (active phase) to NiO_2 and/or γ-NiOOH (less active phase). Nano-CS-NiOOH/GC electrode exhibits a higher stability (i.e., its stability increases slightly with time) towards ORR compared to nano-NiOOH/GC electrode (see Fig. 12B). Additionally, nano-CS-NiOOH/GC electrode show a higher stability (see Fig. S8A) and methanol poisoning tolerance (Fig. S8B) compared to the commercial Pt/C electrode (Fig. S8C).

The electrocatalytic activity of nano-CS-NiOOH/GC electrode increased with the ageing time, as indicated from the positive shift in the onset potential and half-wave potential of $E_{1/2}$ compared with the fresh electrode. Moreover, *E-t* curves of nano-NiOOH/GC and nano-CS-NiOOH/GC electrodes (see inset of Fig. 12B) revealed that the electrocatalytic activity of nano-NiOOH/GC for ORR was significantly decreased with time (more than 400 mV negative shift on the ORR potential after only 10 min) whereas the activity performance of nano-CS-NiOOH/GC electrode remains unchanged. Figs. 11 and 12 depict the high stability of the nano-CS-NiOOH/GC electrode towards Gox, OER and ORR reactions in alkaline medium compared with nano-NiOOH/GC electrode. The significant improvement in its activity and stability is attributed to the chitosan matrix, which stabilizes the active nickel oxyhydroxide phase.

3.5. Glucose electro-sensing: sensitivity and selectivity

Fig. 13A compares the amperometric responses of the nano-CS-NiOOH/GC (curve b) and nano-NiOOH/GC (curve a) electrodes at 0.5 V during the successive addition of a certain glucose concentration into stirred 0.1 N NaOH. The currents for both electrodes rapidly increase after each addition of glucose to the stirred solution achieving 96% steady-state current within 3.5 s (nano-CS-NiOOH/GC) and 6 s (nano-NiOOH/GC), respectively. The sensitivity of the nano-CS-NiOOH/GC electrode (687 μA mM^{-1} cm^{-2}) is 34-fold greater than that obtained at the NiOOH/GC electrode

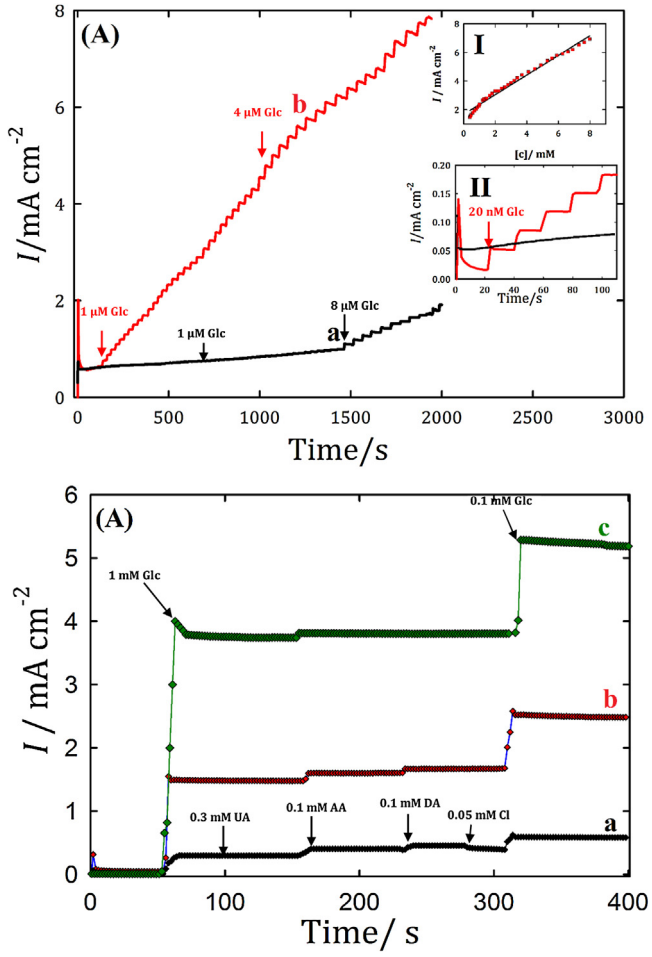

Fig. 13. (A) Amperometric response of the nano-NiOOH/GC (a) and nano-CS-NiOOH/GC (b) electrodes measurement at 0.5 V with successive addition of glucose into 0.1 M NaOH solution (Inset (I) Calibration curve for current density vs. concentration of glucose and (II) zoom of the first five additions). (B) Amperometric response of (a) annealed nano-NiOOH/GC, un-annealed (b) and annealed (c) nano-CS-NiOOH/GC to successive addition of 0.1 mM DA, 0.1 mM AA, 0.3 mM UA, 0.05 M NaCl and 1 mM glucose at an applied potential of 0.48 V.

(20 μA mM^{-1} cm^{-2}) and the detection limit can reach values as low as 0.02 μM and 1.4 μM for nano-CS-NiOOH/GC and nano-NiOOH/GC electrode based on a signal-to-noise ratio of 3 (14 times higher compared with nano-NiOOH/GC electrode with the same weight, see inset II), respectively. Moreover, the linear range has also been greatly improved for the nano-CS-NiOOH/GC electrode, whereas the catalytic current is linear with the glucose concentration up to 8 mM with a coefficient of 0.9987 (see inset I). To estimate the sensing performance of our prepared sensor, a comparison of the nano-CS-NiOOH/GC with other non-enzymatic glucose sensors is listed in Table S2. It can be observed that the detection limit, sensitivity and linear calibration range for glucose detections at nano-CS-NiOOH/GC electrode are comparable with or even better than those obtained with several of the listed electrodes in Table S2. The high sensitivity and low detection limit of nano-CS-NiOOH/GC might be attributed to the CS matrix, which provides a high specific surface area and numerous active sites and also allows the access of analytes to all active catalytic sites with minimal diffusion resistance.

Selectivity is one of the essential features of a high-performance non-enzymatic glucose sensor. In order to evaluate the selectivity of the proposed sensor, four interfering electroactive species which usually coexist with glucose in the real samples, such as ascorbic acid (AA), uric acid (UA), dopamine (DA) and chloride

(might affect the detection of glucose) were investigated at a physiological concentration, considering that the concentrations of chloride ions is about 10 times that of glucose concentration, while the AA and UA are one-tenth of the glucose concentration in the real human bloods. Fig. 13B reveals that the corresponding oxidation current changes are 0.2, 1.68 and 3.89 mA cm^{-2} for nano-NiOOH/GC (curve a), nano-CS-NiOOH/GC (without any heat treatment, curve b) and nano-CS-NiOOH/GC (calcined at 250 °C, curve c) upon adding 1 mM glucose, respectively. This current responses (for these three electrodes) did not get altered in the presence of 0.1 mM UA. This figure also illustrates that the glucose oxidation current at nano-CS-NiOOH/GC electrodes (un-calcined and calcined) was not altered even in the presence of an excess of chloride ions (0.05 M), while nano-NiOOH/GC electrode shows 3.5% decrease in the glucose oxidation current, indicating that nano-CS-NiOOH/GC electrode exhibits a good resistance for surface fouling compared with nano-NiOOH/GC electrode (i.e., effect of NaCl on the sensor material towards glucose were negligible). Adding 0.1 mM of DA and AA resulted in 25% and 13% increase in the glucose oxidation current response of nano-NiOOH/GC electrode, while the same concentrations of these interfering species resulted in only 7% and 2% increases on the glucose response at nano-CS-NiOOH/GC electrode (without heat treatment), indicating the better sensing selectivity of the nano-CS-NiOOH/GC electrode compared with nano-NiOOH/GC electrode. Interestingly, the current response of glucose (1 mM) on calcined nano-CS-NiOOH/GC electrode was not changed even in the presence of other oxidisable species like AA, UA and DA. This might be due to the change of the nickel oxide phase after heat treatment. The only plausible explanation for that finding is that the calcination step resulted in the formation of a new nickel phase which is active for glucose oxidation and less active for AA and DA. The above results indicate that the proposed electrode exhibits good selectivity towards glucose in the presence of common interferents present in blood and is promising for the development of a non-enzymatic glucose sensor.

4. Conclusion

A novel Pt-free catalyst of nano-CS-NiOOH with outstanding electrocatalytic activity and stability for ORR and OER is investigated, for the first time. Nano-CS-NiOOH showed a higher catalytic activity, stability and methanol poisoning tolerance for ORR compared to the commercial Pt/C catalyst. Additionally, nano-CS-NiOOH catalyst exhibited an exceptional activity, selectivity and durability for glucose electrooxidation and electrosensing. The impacts of annealing temperature and nickel loading on the structural and electrocatalytic activity properties of nano-CS-NiOOH/GC electrode were investigated. The calcination temperature of nano-CS-NiOOH played a prominent role for the structural and electrocatalytic activity of the prepared catalysts. The electrocatalytic activity of the nano-CS-NiOOH/GC electrode towards ORR, OER and Gox increases with the increase of calcination temperature (≥280 °C) above this temperature the electrode activity significantly decreased due to the CS matrix destruction. Nano-CS-NiOOH/GC electrode showed higher sensitivity (34-times higher), very low detection limit (20 nM) and selectivity for the detection of glucose, which may be due to the high absorption capacity and huge surface area of the chitosan matrix compared with nano-NiOOH/GC electrode. While β-NiOOH is believed to play a crucial role as a catalytic mediator to facilitate the charge transfer during Gox, ORR and OER reactions, chitosan is thought to enhance the catalytic activity and durability by stabilizing the nickel oxyhydroxide active phase (β-NiOOH) and increasing its surface active sites. Additionally, chitosan is believed to enhance the adsorption of active species through its —NH_2 and —OH like functional groups. We believe that these outstanding properties of nano-CS-NiOOH/GC electrode and its low cost make it a promising material in sensor and fuel cells applications.

Acknowledgements

This work was financially supported by Alexander von Humboldt Foundation (AvH). Gumaa A. El-Nagar is grateful for a fellowship from the AvH.

Appendix A. Supplementary data

Supplementary data associated with this article can be found, in the online version, at http://dx.doi.org/10.1016/j.apcatb.2016.11.031.

References

[1] B. Smitha, S. Sridhar, A.A. Khan, J. Membr. Sci. 259 (2005) 10–26.
[2] Y. Wang, K.S. Chen, J. Mishler, S.C. Cho, X.C. Adroher, Appl. Energy 88 (2011) 981–1007.
[3] Y.-J. Wang, J. Qiao, R. Baker, J. Zhang, Chem. Soc. Rev. 42 (2013) 5768–5787.
[4] G.A. El-Nagar, A.M. Mohammad, M.S. El-Deab, T. Ohsaka, B.E. El-Anadouli, J. Power Sources 265 (2014) 57–61.
[5] B. Machol, S. Rizk, Environ. Int. 52 (2013) 75–80.
[6] H. Liu, D. Liang, Renew. Sustain. Energy Rev. 18 (2013) 486–498.
[7] Y.-L. Yang, X.-H. Liu, M.-Q. Hao, P.-P. Zhang, Int. J. Hydrogen Energy 40 (2015) 10979–10984.
[8] D. Basu, S. Basu, Int. J. Hydrogen Energy 37 (2012) 4678–4684.
[9] D. Basu, S. Basu, J. Solid State Electrochem. 17 (2013) 2927–2938.
[10] D. Basu, S. Basu, Electrochim. Acta 56 (2011) 6106–6113.
[11] Ó. Santiago, E. Navarro, M.A. Raso, T.J. Leo, Appl. Energy 179 (2016) 497–522.
[12] J. Chen, C.X. Zhao, M.M. Zhi, K. Wang, L. Deng, G. Xu, Electrochim. Acta 66 (2012) 133–138.
[13] T. Jiang, L. Yan, Y. Meng, M. Xiao, Z. Wu, P. Tsiakaras, S. Song, Appl. Catal. B: Environ. 162 (2015) 275–281.
[14] A. Brouzgou, L.L. Yan, S.Q. Song, P. Tsiakaras, Appl. Catal. B: Environ. 147 (2014) 481–489.
[15] A. Brouzgou, P. Tsiakaras, Top. Catal. 58 (2015) 1311–1327.
[16] S. Ci, Z. Wen, S. Mao, Y. Hou, S. Cui, Z. He, J. Chen, Chem. Commun. 51 (2015) 9354–9357.
[17] Z. Zhu, F. Sun, X. Zhang, Y.H.P. Zhang, Biosens. Bioelectron. 36 (2012) 110–115.
[18] V. Oncescu, D. Erickson, Sci. Rep. 3 (2013) 1226.
[19] Z. Shen, W. Gao, P. Li, X. Wang, Q. Zheng, H. Wu, Y. Ma, W. Guan, S. Wu, Y. Yu, K. Ding, Talanta 159 (2016) 194–199.
[20] M. Shamsipur, M. Najafi, M.-R.M. Hosseini, Bioelectrochemistry 77 (2010) 120–124.
[21] A.M. Ghonim, B.E. El-Anadouli, M.M. Saleh, Electrochim. Acta 114 (2013) 713–719.
[22] M. Fleischmann, K. Korinek, D. Pletcher, J. Electroanal. Chem. Interfacial Electrochem. 31 (1971) 39–49.
[23] J. Taraszewska, G. Rosłonek, J. Electroanal. Chem. 364 (1994) 209–213.
[24] M. Fleischmann, K. Korinek, D. Pletcher, J. Chem. Soc. Perkin Trans. 2 (1972) 1396–1403.
[25] C. Zhao, C. Shao, M. Li, K. Jiao, Talanta 71 (2007) 1769–1773.
[26] I. Becerik, F. Kadirgan, Electrochim. Acta 37 (1992) 2651–2657.
[27] M. Tominaga, T. Shimazoe, M. Nagashima, I. Taniguchi, Electrochem. Commun. 7 (2005) 189–193.
[28] S.-i. Mho, D.C. Johnson, J. Electroanal. Chem. 500 (2001) 524–532.
[29] H. Mei, Q. Sheng, H. Wu, X. Zhang, S. Wang, Q. Xia, Microchim. Acta 182 (2015) 2395–2401.
[30] G. Wang, X. He, L. Wang, A. Gu, Y. Huang, B. Fang, B. Geng, X. Zhang, Microchim. Acta 180 (2013) 161–186.
[31] A. Bhatnagar, M. Sillanpää, Adv. Colloid Interface Sci. 152 (2009) 26–38.
[32] X. Zhu, A. Ding, Int. J. Electrochem. Sci. 8 (2013) 135–148.
[33] E. Khaled, H.N.A. Hassan, I.H.I. Habib, R. Metelka, Int. J. Electrochem. Sci. 5 (2010) 158–167.
[34] S. Taufik, N.A. Yusof, T.W. Tee, I. Ramli, Int. J. Electrochem. Sci. 6 (2011) 1880–1891.
[35] J. Yang, J.-H. Yu, J. Rudi Strickler, W.-J. Chang, S. Gunasekaran, Biosens. Bioelectron. 47 (2013) 530–538.
[36] L.M. Lu, L. Zhang, F.L. Qu, H.X. Lu, X.B. Zhang, Z.S. Wu, S.Y. Huan, Q.A. Wang, G.L. Shen, R.Q. Yu, Biosens. Bioelectron. 25 (2009) 218–223.
[37] A. Ciszewski, I. Stepniak, Electrochim. Acta 111 (2013) 185–191.
[38] M. Rhazi, J. Desbrières, A. Tolaimate, M. Rinaudo, P. Vottero, A. Alagui, M. El Meray, Eur. Polym. J. 38 (2002) 1523–1530.
[39] I.M.N. Vold, K.M. Vårum, E. Guibal, O. Smidsrød, Carbohydr. Polym. 54 (2003) 471–477.
[40] C. Li, S. Liu, J. Nanomater. 2012 (2012) 6.

[41] D.S. Hall, D.J. Lockwood, C. Bock, B.R. MacDougall, Nickel hydroxides and related materials: a review of their structures, synthesis and properties, Proc. R. Soc. A R. Soc. (2015) 20140792.
[42] P. Oliva, J. Leonardi, J. Laurent, C. Delmas, J. Braconnier, M. Figlarz, F. Fievet, A. De Guibert, J. Power Sources 8 (1982) 229–255.
[43] A.M. Mohammad, G.A. El-Nagar, I.M. Al-Akraa, M.S. El-Deab, B.E. El-Anadouli, Int. J. Hydrogen Energy 40 (2015) 7808–7816.
[44] G.A. El-Nagar, A.M. Mohammad, M.S. El-Deab, B.E. El-Anadouli, Electrochim. Acta 94 (2013) 62–71.
[45] S. Stevanović, V. Panić, D. Tripković, V.M. Jovanović, Electrochem. Commun. 11 (2009) 18–21.
[46] Y.B. Vassilyev, O.A. Khazova, N.N. Nikolaeva, J. Electroanal. Chem. 196 (1985) 127–144.
[47] M.W. Hsiao, R.R. Adzic, E.B. Yeager, Electrochim. Acta 37 (1992) 357–363.
[48] A.C. de Sá, L.L. Paim, N.R. Stradiotto, Int. J. Electrochem. Sci. 9 (2014) 7746–7762.
[49] S. Berchmans, H. Gomathi, G.P. Rao, J. Electroanal. Chem. 394 (1995) 267–270.
[50] A.J. Bard, L.R. Faulkner, J. Leddy, C.G. Zoski, Electrochemical Methods: Fundamentals and Applications, Wiley New York, 1980.
[51] C. Song, J. Zhang, PEM Fuel Cell Electrocatalysts and Catalyst Layers: Fundamentals and Applications, in: J. Zhang (Ed.), Springer London, London, 2008, pp. 89–134.
[52] F. He, Y. Chen, P. Zhao, S. Liu, J. Nanopart. Res. 18 (2016) 119.
[53] A.S. Danial, M.M. Saleh, S.A. Salih, M.I. Awad, J. Power Sources 293 (2015) 101–108.
[54] B. Mondal, L. Dutta, C. Roychaudhury, D. Mohanta, N. Mukherjee, H. Saha, Acta Metall. Sin. (English Letters) 27 (2014) 593–600.
[55] C.W.B. Bezerra, L. Zhang, H. Liu, K. Lee, A.L.B. Marques, E.P. Marques, H. Wang, J. Zhang, J. Power Sources 173 (2007) 891–908.
[56] Y.G. Ko, H.J. Lee, S.S. Shin, U.S. Choi, Soft Matter 8 (2012) 6273–6279.